Fano Resonances in the Infrared Spectra of Phonons in Hyperkagome $Na_3Ir_3O_8$

D. Pröpper,[1] A. N. Yaresko,[1] T. I. Larkin,[1] T. N. Stanislavchuk,[2] A. A. Sirenko,[2] T. Takayama,[1,3] A. Matsumoto,[1,3] H. Takagi,[1,3] B. Keimer,[1] and A. V. Boris[1]

[1]*Max-Planck-Institut für Festkörperforschung, Heisenbergstraße 1, D-70569 Stuttgart, Germany*

[2]*Department of Physics, New Jersey Institute of Technology, Newark, New Jersey 07102, USA*

[3]*Department of Physics, University of Tokyo, Hongo, Tokyo 113-0033, Japan*

(Received 8 November 2013; published 26 February 2014)

We report the complex dielectric function of high-quality $Na_3Ir_3O_8$ single crystals determined by spectroscopic ellipsometry in the spectral range from 15 meV to 2 eV. The far-infrared phonon spectra exhibit highly asymmetric line shapes characteristic of Fano resonances. With decreasing temperature, we observe a sharp increase of the infrared intensity of the Fano-shaped phonon modes accompanied by concomitant changes in the low-energy electronic background, formed by electronic transitions between Ir $5d$ t_{2g} bands of a mostly $J_{\mathrm{eff}} = 1/2$ character. The role of the complex hyperkagome lattice structure and strong spin-orbit coupling is considered.

DOI: 10.1103/PhysRevLett.112.087401 PACS numbers: 78.20.Ci, 63.20.kd, 71.70.Ej, 71.20.-b

The electronic states near the Fermi energy of transition metal oxides with $5d$ valence electrons, compared to their $3d$-electron counterparts, exhibit larger single-electron bandwidths, reduced on-site Coulomb correlations, and enhanced spin-orbit coupling (SOC). The convergence of these three energy scales has been proposed to give rise to novel electronic phases, including relativistic Mott insulators with antiferromagnetic [1–3] and spin liquid [4–9] ground states, for geometrically unfrustrated and frustrated lattices, respectively. Despite the prominent role of the electron-phonon (e-ph) interaction in the physics of $3d$-electron analogues (including especially those with orbital degeneracy and geometrically frustrated lattice architectures [10]), its influence on the electronic properties and phase behavior of $5d$-electron compounds has not yet been addressed.

One of the most striking manifestations of the electron-phonon interaction is the quantum interference between discrete phonons and the continuum of electron-hole excitations, which leads to asymmetric Fano resonances [11,12] in the scattering and infrared (IR) absorption spectra of solids [13,14]. As the electronic contribution increases, the Fano resonance may undergo a change from a phonon absorption peak to a pronounced dip corresponding to reduced absorption. This dramatic behavior is one of the characteristic properties of few-layer graphene where Fano resonances have been recently observed and studied in detail [15–21]. This elementary solid with tunable electron density has proved to be a model system to develop a microscopic theory that accounts quantitatively for the intensity and asymmetry of the Fano resonances [20,21].

In this Letter, we provide evidence that conditions favorable for Fano interference are met in $Na_3Ir_3O_8$, the semimetallic counterpart of Mott-insulating $Na_4Ir_3O_8$, one of the best candidates for a three-dimensional (3D) spin-liquid state [10]. In both $Na_3Ir_3O_8$ and $Na_4Ir_3O_8$, Ir ions are arranged on a three-dimensional geometrically frustrated hyperkagome lattice. In formal analogy to the single-band Hubbard model [1], one refers to the $J_{\mathrm{eff}} = 1/2$ spin-orbit $5d$ t_{2g} states of $Na_4Ir_3O_8$ as a half-filled narrow Mott-Hubbard band [22–28], which becomes one-third filled in semimetallic $Na_3Ir_3O_8$. We discovered that the entire set of well-defined phonon modes in the ellipsometric IR spectra of our $Na_3Ir_3O_8$ single crystals exhibits highly asymmetric line shapes characteristic of Fano resonances. We show that with decreasing temperature a sharp increase of the Fano resonances is accompanied by concomitant changes in the underlying low-energy electronic transitions. On the basis of fully relativistic electronic-structure calculations in the local density approximation (LDA), we attribute this unusual behavior to Rashba-type Ir $5d$ t_{2g} bands intersecting near the Fermi level (resembling the Dirac cone in graphene). These bands originate from strong SOC combined with the broken inversion symmetry of the cubic lattice.

Single crystals $Na_3Ir_3O_8$ of approximate dimensions $0.3 \times 0.5 \times 0.5$ mm^3 were grown from NaCl flux [29]. They crystallize in a cubic structure described by space groups $P4_132$ or $P4_332$ (No. 213 and No. 212 in the international tables for x-ray crystallography, respectively), with 4 formula units/unit cell [see Fig. 1(a)]. X-ray diffraction analysis indicates that 12 Na atoms per unit cell sit in two fully occupied nonequivalent positions marked as Na^{I} and Na^{II} in Fig. 1(a). This cubic structure can be regarded as a distorted modification of the face-centered cubic $2 \times NaIr_2O_4$ pyrochlore structure with space group $Fd\bar{3}m$, where a Na^{I} ion replaces one of the four Ir sites in the 3D pyrochlore corner-sharing tetrahedron lattice $2 \times Na(Na_{1/2}Ir_{3/2})O_4$.

We report a spectroscopic ellipsometry study of $Na_3Ir_3O_8$ over a wide range of temperatures (8–300 K) and photon energies extending from the far IR into the

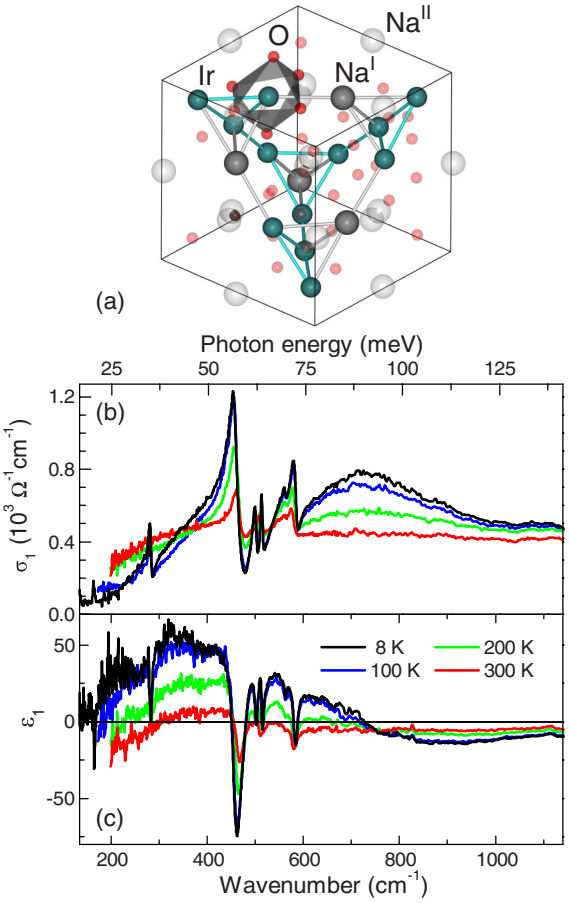

FIG. 1 (color online). (a) Crystal structure of $Na_3Ir_3O_8$ with the space group $P4_132$. Intertwined Ir_3Na tetrahedra form a hyperkagome sublattice of Ir ions. Oxygen atoms occupy the corners of distorted octahedra around the Ir and Na^I sites. [(b) and (c)] Real part of the IR (b) conductivity $\sigma_1(\omega)$ and (c) dielectric permittivity $\varepsilon_1(\omega)$.

visible range, from 15 meV to 2 eV. Experimental details can be found in Refs. [30,31]. The complex dielectric function $\tilde{\varepsilon}(\omega) = \varepsilon_1(\omega) + i\varepsilon_2(\omega)$ and the related optical conductivity $\sigma_1(\omega) = \omega\varepsilon_2(\omega)/(4\pi)$ were determined by direct inversion of the Fresnel equations from the ellipsometric parameters $\Psi(\omega)$ and $\Delta(\omega)$.

Figures 1(b) and 1(c) show variation with temperature of the real part of the optical conductivity $\sigma_1(\omega)$ and permittivity $\varepsilon_1(\omega)$, respectively, in the spectral range from 120 to 1200 cm^{-1} (15–150 meV). The low-energy cutoff is determined by the sample dimensions and caused by the polarization-dependent diffraction of infrared light resulting in uncertainty in the analysis of the ellipsometric parameters [32]. In the low-T spectrum one can identify a set of seven highly asymmetric phonon modes located at 166, 281, 461, 501, 514, 562, and 583 cm^{-1}. Following the Wyckoff positions of the 56 atoms and their site symmetries in the $P4_132$ unit cell of $Na_3Ir_3O_8$ one would expect 21 triply degenerated T_1 IR-active modes [33]. Only seven of these modes are observed in the spectra. This is most likely due to insufficient strength and/or weak splitting of the four T_{1u} modes in the assumptive parent $Fd\bar{3}m$ pyrochlore structure of $NaIr_2O_4$. The observed asymmetric modes are superimposed on a humplike absorption band centered around 728 cm^{-1} (90 meV), which grows monotonously in intensity on an almost flat background upon cooling. The downturn in ε_1 below 360 cm^{-1} (45 meV) indicates the free charge carrier response. In order to reconcile the IR and dc conductivity data [29], we introduce a narrow and weak single Drude peak with the plasma frequency $\omega_{pl} \lesssim 0.2$ eV. The corresponding effective charge carrier density $N^{eff} = [2m/(\pi e^2 N_{Ir})](\omega_{pl}^2/8) \approx 0.002\ e$ per Ir atom, where m is the free electron mass and $N_{Ir} = 1.65 \times 10^{22}$ cm^{-3} is the density of Ir atoms.

In order to quantitatively parametrize the observed highly asymmetric far-IR modes and the strongly temperature-dependent electronic background, we fit a set of generalized Lorentzian oscillators [34] simultaneously to $\varepsilon_1(\omega)$ and $\varepsilon_2(\omega)$

$$\varepsilon_1(\omega) + i\varepsilon_2(\omega) = \varepsilon_\infty + \sum_{j=1}^{K} \frac{\Delta\varepsilon_j(\omega_j^2 - i\omega\beta_j)}{\omega_j^2 - \omega^2 - i\omega\gamma_j} \qquad (1)$$

with ω_j, γ_j, and β_j the resonance frequency, line width, and asymmetry parameter, respectively, having dimensions of frequency and dimensionless $\Delta\varepsilon_j$ being the contribution to the static permittivity. The interband transitions at high energies contribute to the background term ε_∞. The causality of the dielectric response and Kramers-Kronig requirements over the entire spectral range are maintained by holding the condition of

$$\sum_j \Delta\varepsilon_j\beta_j = 0. \qquad (2)$$

Figures 2(a) and 2(b) and Table I summarize the results of our dispersion analysis of the complex dielectric function measured at 8 K. The noticeable deviation of the fit of ε_1 from the data at low frequency is caused by the simplified single Drude peak description we used for the charge carrier response in this strongly coupled multiband material. At the same time, we unambiguously identify seven phonon modes that are highly asymmetric as indicated by the large, negative $\beta_j^{(ph)}$ value. In order to maintain the condition of Eq. (2) we used the same model with nonzero parameter $\beta_j^{(e)}$ in Eq. (1) for one of the low-energy electronic bands but with the opposite sign compensating the high-energy contributions of the phonon modes. Since the spectral weight (SW) of broad electronic transitions is large compared to that of the phonon modes, the asymmetry parameter $\beta_j^{(e)} > 0$ is relatively small and cannot be unequivocally assigned to one or another of the constituent optical bands of the electronic background. In the representative fit shown in Figs. 2(a) and 2(b) the optical band at 358 cm^{-1} (44 meV) was selected to be asymmetric with $\beta_1^{(e)} = 97$, whereas the band at 728 cm^{-1} (90 meV) was

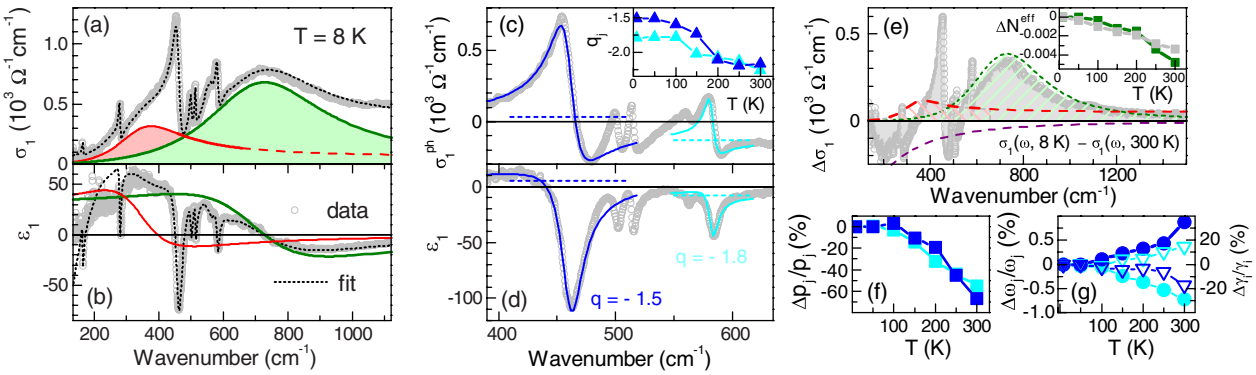

FIG. 2 (color online). Real part of the IR (a) conductivity $\sigma_1(\omega)$ and (b) dielectric permittivity $\varepsilon_1(\omega)$ measured at $T = 8$ K (open circles) and represented by the fit to the coupled oscillator model with Eq. (1) (dashed lines) and by the partial contribution of the low-energy electronic transitions [(a) shaded areas, (b) solid lines]. [(c) and (d)] Examples of the Fano fit to the spectra in the region of the phonon modes at 461 cm^{-1} (dark blue) and 583 cm^{-1} (light cyan), obtained by subtraction of an electronic background from the data in (a) and (b). Inset: Temperature dependence of the corresponding Fano coupling parameters q_j. (e) Difference spectra $\sigma_1(8\text{ K}, \omega) - \sigma_1(300\text{ K}, \omega)$ (open circles) represented by the changes in the separate absorption bands (dashed lines). Inset: The SW difference with increasing temperature, integrated up to 0.5 eV (light squares), along with the changes in the strength of the optical band at 728 cm^{-1} (90 meV) (dark squares) as derived from the fits. [(f) and (g)] Relative changes in the Fano parameters with increasing temperature: (f) strength p_j and (g) resonance frequency ω_j (solid circles) and width γ_j (open triangles) for the representative modes at 461 cm^{-1} (dark blue) and 583 cm^{-1} (light cyan).

taken to be a classical Lorentz oscillator with $\beta_2^{(e)} = 0$. Some uncertainty of the phenomenological fitting procedure in the determination of the asymmetry parameter $\beta_j^{(e)}$ does not affect the parameters of the phonon modes listed in Table I. In the vicinity of the resonance frequency, the generalized Lorentz oscillator in Eq. (1) can be converted into the Fano profile resulting from the quantum interference of a discrete state with a continuum

$$\Delta\sigma_1^j(\omega) = \sigma_0^j \frac{(q_j + \varepsilon)^2}{1 + \varepsilon^2}, \tag{3}$$

where $\varepsilon = 2(\omega - \omega_j)/\gamma_j$ and $(2\omega_j q_j)/(q_j^2 - 1) \approx \beta_j$ [34]. Figures 2(c) and 2(d) illustrate exemplarily the Fano profiles for the two strongest resonances at $T = 8$ K. Both resonances are characterized by $q \approx -1.5$ with an antisymmetric absorption line shape implying comparable phonon and electronic contributions into the Fano resonances. The temperature evolution of q_j is shown in the inset of Fig. 2(c), and one can see that the electron-phonon coupling weakens with increasing temperature.

Figure 2(e) displays the changes occurring in the IR conductivity spectra with increasing temperature, as shown by the difference spectra $\Delta\sigma_1(\omega) = \sigma_1(\omega, 8\text{ K}) - \sigma_1(\omega, 300\text{ K})$. By using the dispersion analysis of the dielectric function spectra at different temperatures with Eq. (1), we determine more accurately the temperature variation of the constituent Drude and low-energy interband contributions shown by the dashed lines in Fig. 2(e). The corresponding loss of the associated SW, $SW_j = (\pi/120)\Delta\varepsilon_j\omega_j^2$, with increasing temperature above 8 K is detailed in the inset of Fig. 2(e) for the optical band at 728 cm^{-1} (90 meV), along with the temperature dependence of the integrated SW difference $\Delta SW(T) = \int_0^{1\text{ eV}} [\sigma_1(\omega, T) - \sigma_1(\omega, 8\text{ K})]d\omega$. In the latter case, the SW in the extrapolation region below 15 meV was determined by the procedure based on the Kramers-Kronig consistency check of the experimentally measured $\Delta\varepsilon_1(\omega)$ and $\Delta\sigma_1(\omega)$, 15 meV $< \omega <$ 1 eV (see Methods in Ref. [30]). The temperature-driven loss of the SW, expressed in terms of the effective number of charge carriers $\Delta N^{\text{eff}}(T) = [2m/(\pi e^2 N_{\text{Ir}})]\Delta SW$, is comparable to the free carrier density evaluated above, and it is not recovered within a high-energy scale in excess of 1 eV. In order to quantify the temperature-dependent intensity of the sharp Fano resonances we refer to the strength parameter p_j [20], which accounts for its both positive and negative contributions to $\Delta\sigma_1^j(\omega)$ (approximately equal for $q_j \approx 1$): $p_j = \Delta\varepsilon_j\omega_j^2(1 + 1/q_j^2)/8$. Figure 2(f) shows the temperature evolution of the Fano-strength parameter p_j for the two representative resonances. It appears clear from our

TABLE I. Best-fit results for the Fano resonances and low-energy electronic transitions in the far-IR spectral range of $Na_3Ir_3O_8$ at $T = 8$ K with ω_j, $\Delta\varepsilon_j$, γ_j, β_j, and q_j being the resonance frequency, contribution to the static permittivity, line width, and asymmetry parameters, respectively.

	j	ω_j (cm^{-1})	$\Delta\varepsilon_j$	γ_j (cm^{-1})	β_j (cm^{-1})	q_j
(ph)	1	166	0.70	3.0	−101	−3.6
	2	281	0.56	5.0	−535	−1.7
	3	461	2.33	22.6	−1092	−1.5
	4	501	0.33	6.8	−490	−2.5
	5	514	0.27	4.3	−318	−3.5
	6	562	0.05	7.3	−400	−3.1
	7	583	0.31	8.9	−950	−1.8
(e)	1	358	36.1	249	97	7.4
	2	728	34.4	447		

analysis that both the intensity and Fano-asymmetry variations of the sharp resonances correlate remarkably well with the strength of the underlying electronic transitions. Therefore, the SW loss of the phonon resonances stems from the SW loss of the interband transition. The observed intensity and asymmetry (Table I) of the Fano resonances imply a considerable e-ph coupling in $Na_3Ir_3O_8$, given the high bonding ionicity and the large number of IR active modes with evidently large intrinsic dipole moments. This is in stark contrast to the case of graphene, where the static intrinsic dipole is negligible and similar values of the Fano parameter q [15–19] originate mainly from the electronic excitations in the presence of a relatively small e-ph coupling [20]. Further evidence for the strong interaction of the phonons with the underlying electronic transitions in $Na_3Ir_3O_8$ is the temperature dependence of the resonance frequency and width of the strongest mode at 461 cm^{-1} [dark solid circles and open triangles in Fig. 2(g), respectively], which hardens and narrows with increasing temperature. A quantitative estimate of the e-ph coupling constants and the Born effective charges requires a detailed analysis of the lattice dynamics in this complex hyperkagome structure, which is an important challenge for future theoretical work.

We take the first step in this direction by identifying the origin of the electronic bands coupled to the phonons and performed relativistic LDA band structure calculations using the linear muffin-tin orbital method [35,36] for the experimental crystal structure of $Na_3Ir_3O_8$ [29]. Although the IrO_6 octahedra are distorted, the Ir d shell is split into well separated "t_{2g}" and "e_g" states. A simple electron count shows that the t_{2g} states of each Ir are filled by 4.67 e. Despite the noninteger valency of an $Ir^{4.33+}$ ion, scalar-relativistic calculations that neglect SOC give an insulating solution with eight unoccupied bands separated by a gap of ~0.2 eV from the remaining occupied t_{2g} bands. Fully relativistic Ir t_{2g} bands decorated with circles proportional to the weight of Ir $d_{3/2}$ and $d_{5/2}$ states are shown in Fig. 3(c). Since the crystal structure lacks inversion symmetry, the Kramers degeneracy is lifted everywhere except for time-reversal invariant points. A striking effect of strong SOC is that a pair of unoccupied t_{2g} bands closes the gap [green lines in Fig. 3(d)] and creates two large electronlike Fermi surfaces around the R point. The charge balance is then maintained by depopulating holelike bands near Γ [red lines in Fig. 3(d)] rendering the material semimetallic, with a negative indirect band gap between Γ and R. In semimetallic materials, strong temperature effects in the optical spectra are expected [37]. As temperature increases, the phonon assistance of the indirect transitions is dramatically enhanced, which changes the valence and conduction band occupancies at the R and Γ points, respectively. This may explain the observed temperature evolution of the low-energy electronic background with its spectral weight redistribution over an extended energy range.

The relativistic t_{2g} bands are subdivided into a lower- and a higher-energy group reflecting the splitting of Ir t_{2g} states

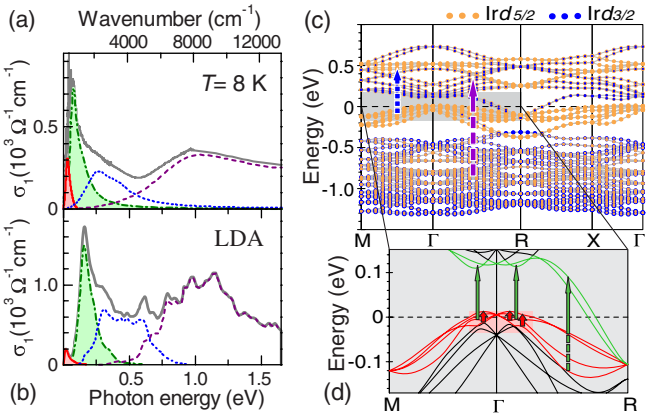

FIG. 3 (color online). (a) $\sigma_1(\omega)$ of $Na_3Ir_3O_8$ measured at T = 8 K and contributing interband transitions determined by a dispersion analysis. (b) Corresponding relativistic LDA calculation with a breakdown into separate t_{2g} orbital contributions. (c) Band structure for Ir t_{2g} states. The size of blue and orange circles is proportional to the weight of d states with true $d_{3/2}$ and $d_{5/2}$ orbital character, respectively. (d) Enlargement of the band structure of (c). Color coding sketched with arrows in (c) and (d) corresponds to the band color in (a) and (b).

into a quartet with $J_{\rm eff} = 3/2$ and a doublet with $J_{\rm eff} = 1/2$. As compared to $Na_4Ir_3O_8$ [22–28], the filling of the $J_{\rm eff} = 1/2$ states is significantly reduced from one-half to one-third and, therefore, one would expect that the renormalization of the Ir t_{2g}-derived bands due to correlation effects is strongly suppressed. As the functions of the $J_{\rm eff} = 1/2$ doublet are given by linear combinations of $d_{5/2}$ states only, the appreciable contribution of $d_{3/2}$ states to unoccupied t_{2g} bands [Fig. 3(c)] implies a strong hybridization between the $J_{\rm eff} = 3/2$ and $J_{\rm eff} = 1/2$ states. These transitions are responsible for a peak of the optical conductivity below 0.1 eV shaded by red in Fig. 3(b). The bands crossing E_F also provide an intraband Drude contribution to the conductivity with $\omega_{\rm pl} = 0.6$ eV [not shown in Fig. 3(b)], which is somewhat larger than the experimentally observed value. A sharp peak at 0.2 eV (green shaded area) is due to interband transitions from occupied $J_{\rm eff} = 1/2$ bands to the pair of bands that cross E_F near R, whereas transitions from the same initial $J_{\rm eff} = 1/2$ bands to the rest of the unoccupied t_{2g} bands give a broad feature centered at 0.5 eV. Finally, transitions from the bands formed predominantly by $J_{\rm eff} = 3/2$ states to unoccupied t_{2g} bands give a broad maximum of the conductivity at ~1.2 eV. The overall shape of the optical conductivity, i.e., a strong, low-lying transition followed by a near-IR band peaking at about 1 eV and an absorption edge setting in between 2 and 3 eV, is nicely captured by our calculations, although the absolute values calculated exceed the experimental ones roughly by a factor of 2.

The results presented above emphasize the significance of the e-ph interaction in strongly spin-orbit-driven systems. Because of the lack of inversion symmetry, the four $J_{\rm eff} = 1/2$ bands in $Na_3Ir_3O_8$ have linear Rashba-type dispersion in the vicinity of Γ with their apex lying slightly

above E_F, similar to the bulk band structure of BiTeI [38,39]. An analysis of the dipole matrix elements has shown that interband transitions between these partially filled bands have a high probability. This provides a high density of electron-hole excitations that interfere with superimposed discrete phonon states, in a similar manner as discussed for graphene [15,16]. Our experiments highlight the need for a detailed analysis of the electron-phonon interaction and its influence on the ground states and low-energy excitation spectra in the 5*d*-electron compounds.

We gratefully acknowledge M. Höppner for helpful discussion, Y.-L. Mathis for support at the IR1 beam line of the synchrotron facility ANKA at the Karlsruhe Institute of Technology, and G. L. Carr for support at the U4IR beam line of the NSLS synchrotron at the Brookhaven National Laboratory. The NSLS is operated as a User Facility for the U.S. Department of Energy under Grant No. DE-AC02-98CH10886.

[1] B. J. Kim, H. Jin, S. J. Moon, J.-Y. Kim, B.-G. Park, C. S. Leem, J. Yu, T. W. Noh, C. Kim, S.-J. Oh, J.-H. Park, V. Durairaj, G. Cao, and E. Rotenberg, Phys. Rev. Lett. **101**, 076402 (2008).
[2] B. J. Kim, H. Ohsumi, T. Komesu, S. Sakai, T. Morita, H. Takagi, and T. Arima, Science **323**, 1329 (2009).
[3] J. Kim, D. Casa, M. H. Upton, T. Gog, Y.-J. Kim, J. F. Mitchell, M. van Veenendaal, M. Daghofer, J. van den Brink, G. Khaliullin, and B. J. Kim, Phys. Rev. Lett. **108**, 177003 (2012).
[4] G. Jackeli and G. Khaliullin, Phys. Rev. Lett. **102**, 017205 (2009).
[5] A. Shitade, H. Katsura, J. Kuneš, X.-L. Qi, S.-C. Zhang, and N. Nagaosa, Phys. Rev. Lett. **102**, 256403 (2009).
[6] S. K. Choi, R. Coldea, A. N. Kolmogorov, T. Lancaster, I. I. Mazin, S. J. Blundell, P. G. Radaelli, Y. Singh, P. Gegenwart, K. R. Choi, S.-W. Cheong, P. J. Baker, C. Stock, and J. Taylor, Phys. Rev. Lett. **108**, 127204 (2012).
[7] R. Comin, G. Levy, B. Ludbrook, Z.-H. Zhu, C. N. Veenstra, J. A. Rosen, Y. Singh, P. Gegenwart, D. Stricker, J. N. Hancock, D. van der Marel, I. S. Elfimov, and A. Damascelli, Phys. Rev. Lett. **109**, 266406 (2012).
[8] H. Gretarsson, J. P. Clancy, X. Liu, J. P. Hill, E. Bozin, Y. Singh, S. Manni, P. Gegenwart, J. Kim, A. H. Said, D. Casa, T. Gog, M. H. Upton, H.-S. Kim, J. Yu, V. M. Katukuri, L. Hozoi, J. van den Brink, and Y.-J. Kim, Phys. Rev. Lett. **110**, 076402 (2013).
[9] Y. Okamoto, M. Nohara, H. Aruga-Katori, and H. Takagi, Phys. Rev. Lett. **99**, 137207 (2007).
[10] L. Balents, Nature (London) **464**, 199 (2010).
[11] U. Fano, Phys. Rev. **124**, 1866 (1961).
[12] A. E. Miroshnichenko, S. Flach, and Y. S. Kivshar, Rev. Mod. Phys. **82**, 2257 (2010).
[13] J. Wagner and M. Cardona, Phys. Rev. B **32**, 8071 (1985).
[14] M. J. Rice, N. O. Lipari, and S. Strässler, Phys. Rev. Lett. **39**, 1359 (1977).
[15] A. B. Kuzmenko, L. Benfatto, E. Cappelluti, I. Crassee, D. van der Marel, P. Blake, K. S. Novoselov, and A. K. Geim, Phys. Rev. Lett. **103**, 116804 (2009).
[16] T.-T. Tang, Y. Zhang, C.-H. Park, B. Geng, C. Girit, Z. Hao, M. C. Martin, A. Zettl, M. F. Crommie, S. G. Louie, Y. R. Shen, and F. Wang, Nat. Nanotechnol. **5**, 32 (2010).
[17] Z. Liu, X. Lu, P. Peng, W. Wu, S.-S. Pei, Q. Yu, and J. Bao, Phys. Rev. B **82**, 155435 (2010).
[18] Z. Li, C. H. Lui, E. Cappelluti, L. Benfatto, K. F. Mak, G. L. Carr, J. Shan, and T. F. Heinz, Phys. Rev. Lett. **108**, 156801 (2012).
[19] C. H. Lui, E. Cappelluti, Z. Li, and T. F. Heinz, Phys. Rev. Lett. **110**, 185504 (2013).
[20] E. Cappelluti, L. Benfatto, and A. B. Kuzmenko, Phys. Rev. B **82**, 041402 (2010).
[21] E. Cappelluti, L. Benfatto, M. Manzardo, and A. B. Kuzmenko, Phys. Rev. B **86**, 115439 (2012).
[22] M. J. Lawler, H.-Y. Kee, Y. B. Kim, and A. Vishwanath, Phys. Rev. Lett. **100**, 227201 (2008).
[23] M. J. Lawler, A. Paramekanti, Y. B. Kim, and L. Balents, Phys. Rev. Lett. **101**, 197202 (2008).
[24] Y. Zhou, P. A. Lee, T.-K. Ng, and F.-C. Zhang,, Phys. Rev. Lett. **101**, 197201 (2008).
[25] D. Podolsky, A. Paramekanti, Y. B. Kim, and T. Senthil, Phys. Rev. Lett. **102**, 186401 (2009).
[26] T. Micklitz and M. R. Norman, Phys. Rev. B **81**, 174417 (2010).
[27] M. R. Norman and T. Micklitz, Phys. Rev. B **81**, 024428 (2010).
[28] D. Podolsky and Y. B. Kim, Phys. Rev. B **83**, 054401 (2011).
[29] T. Takayama, A. Matsumoto, J. Nuss, A. Yaresko, K. Ishii, M. Yoshida, J. Mizuki, and H. Takagi, arXiv:1311.2885.
[30] A. Charnukha, P. Popovich, Y. Matiks, D. L. Sun, C. T. Lin, A. N. Yaresko, B. Keimer, and A. V. Boris, Nat. Commun. **2**, 219 (2011).
[31] T. N. Stanislavchuk, T. D. Kang, P. D. Rogers, E. C. Standard, R. Basistyy, A. M. Kotelyanskii, G. Nita, T. Zhou, G. L. Carr, M. Kotelyanskii, and A. A. Sirenko, Rev. Sci. Instrum. **84**, 023901 (2013).
[32] J. Humlíček and C. Bernhard, Thin Solid Films **455–456**, 177 (2004).
[33] E. Kroumova, M. Aroyo, J. Perez-Mato, A. Kirov, C. Capillas, S. Ivantchev, and H. Wondratschek, Phase Transit. **76**, 155 (2003).
[34] J. Humlíček, R. Henn, and M. Cardona, Phys. Rev. B **61**, 14554 (2000).
[35] O. K. Andersen, Phys. Rev. B **12**, 3060 (1975).
[36] V. N. Antonov, B. N. Harmon, and A. N. Yaresko, *Electronic Structure and Magneto-Optical Properties of Solids* (Kluwer Academic Publishers, Dordrecht, 2004).
[37] D. Menzel, P. Popovich, N. N. Kovaleva, J. Schoenes, K. Doll, and A. V. Boris, Phys. Rev. B **79**, 165111 (2009).
[38] K. Ishizaka *et al.*, Nat. Mater. **10**, 521 (2011).
[39] J. S. Lee, G. A. H. Schober, M. S. Bahramy, H. Murakawa, Y. Onose, R. Arita, N. Nagaosa, and Y. Tokura, Phys. Rev. Lett. **107**, 117401 (2011).